Int J Clin Exp Pathol 2023;16(10):260-281
www.ijcep.com /ISSN:1936-2625/IJCEP0150556

Original Article

Immune-related gene prognostic index (IRGPI) for lung adenocarcinoma predicts patient prognosis and immunotherapy response

Zheng Zhu[1*], Wei Feng[1*], Xiao-Yan Tan[1], Pin-Chao Gu[1], Wei Song[2], Hai-Tao Ma[1]

[1]Department of Thoracic Surgery, Suzhou Dushu Lake Hospital (Dushu Lake Hospital Affiliated to Soochow University, Medical Center of Soochow University), Soochow University, No. 9 Chongwen Road, Suzhou 215000, Jiangsu, China; [2]Emergency Department, Suzhou Dushu Lake Hospital (Dushu Lake Hospital Affiliated to Soochow University, Medical Center of Soochow University), Soochow University, No. 9 Chongwen Road, Suzhou 215000, Jiangsu, China. [*]Equal contributors and co-first authors.

Received April 5, 2023; Accepted August 28, 2023; Epub October 15, 2023; Published October 30, 2023

Abstract: Objective: We searched for a predictive biomarker that also predicts whether patients would benefit from immune checkpoint blockade (ICB) treatment from a few angles, because existing biomarkers no longer wholly replicate the interconnections of distinctive elements in the tumor microenvironment (TME). Methods: We identified 55 pivotal IRGs by performing a WGCNA and univariate Cox regression analysis on a lung adenocarcinoma dataset from the TCGA database. The IRGPI model was then constructed using multivariate Cox regression analysis, which identified 16 genes and verified the use of the GSE68465 database. The AUC of the IRGPI was compared to those of the current biomarkers to determine its predictive potential. Then we examined the molecular and immunological properties of ICB and assessed its effectiveness using CTLA4 expression and TIDE. Results: Patients with a high IRGPI had a later clinical stage, more severe symptoms, and a worse prognosis. Patients with a low IRGPI had a higher immune escape potential and were less responsive to immunotherapy. Conclusion: The IRGPI may be a biomarker for determining the prognosis of patients and whether they respond favorably to ICB therapy.

Keywords: Lung adenocarcinoma, immune-related genes, prognosis, immunotherapy, tumor microenvironment

Introduction

One leading cause of mortality from lung cancer is lung adenocarcinoma (LUAD), with greater than 1 million deaths worldwide each year [1]. According to current clinical guidelines, Low-Dose spiral Computed Tomography (LDCT) is recommended for lung cancer screening in high-risk populations. With the popularization of LDCT, a growing range of patients with LUAD have been identified early and have undergone complete resection, which has improved the prognosis. The gold standard for the diagnosis of lung adenocarcinoma is pathologic testing by obtaining a biopsy or cytologic examination [2]. In clinical work, lung adenocarcinoma can be diagnosed by morphologic features under a light microscope [3, 5].

Current clinical treatments for LUAD include surgery, chemotherapy, radiotherapy, immunotherapy, and molecularly-targeted agents. The higher the clinical stage of the patients, the worse the prognosis and survival rate. The 5-year survival rate for patients with stage IA is as high as 95%, while the survival rate for those with stage III-IV lung adenocarcinoma typically falls below 40%.

In addition to traditional radiotherapy and chemotherapy, the use of immune checkpoint inhibitors (ICIs) and molecular targeted treatment has also dramatically improved the prognosis of patients with advanced and metastatic LUAD [4, 6]. However, because of treatment resistance, tumor heterogeneity, and metastasis, the prognosis of LUAD patients still should be improved [7]. Investigating biomarkers for immunotherapy and optimizing combination therapy are urgently needed to provide a better prognosis for patients with LUAD in the future.

An emerging anticancer treatment called immune checkpoint blockade (ICB) therapy

boosts the antitumor immune response by using T-cell regulatory pathways. ICB particularly targets and destroys inhibitory pathways that obstruct efficient antitumor T-cell responses, as opposed to stimulating the immune system to assault targets on tumor cells [8, 10]. ICB therapy has been proven to improve the prognosis of sufferers from a range of tumor types [11]. Although ICB therapy has extensive scientific efficacy, its efficacy varies from patient to patient, especially in patients with LUAD [12]. However, the interactions of various elements in the tumor microenvironment and the response of malignancies to immunotherapy from a single viewpoint, including expression of ligand or gene mutation, may only be partially represented by current biomarkers, such as PD-L1, CTLA4, and tumor mutational burden (TMB).

An immune-associated gene prognosis index was developed based on our research into genes connected to the immune-related gene prognostic index (IRGPI). In regard to accurately forecasting the effectiveness and prognosis of ICB patients, the established model is significantly above the other models now in use. In addition, we noticed that the clinical characteristics, immunophenotype, and immunological characteristics of the various IRGPI subgroups were significantly different from one another, which conferred an ability of IRGPI to differentiate between symptoms that are associated with LUAD patients.

Materials and methods

Data acquisition and design of experiment

The TCGA database (https://portal.gdc.cancer.gov/) was used to retrieve the gene sequencing information of 598 LUAD patients (539 = tumor; 59 = normal) and clinical data of 522 LUAD patients. Then, we retrieved the gene expression and survival data of 443 LUAD samples (GEO: GSE68465) by using the GEO database (https://www.ncbi.nlm.nih.gov/geo/). Inclusion criteria were: (1) patients whose lung adenocarcinoma was determined based on biopsy; (2) tissue samples with complete gene expression data; (3) patients with complete clinical information, including gender, age, clinical stage, TNM stage, survival time, survival status and other relevant details for follow-up research. The exclusion criteria were as follows: (1) patients with missing or unknown clinical information; (2) patients with a history of other malignant tumors; (3) patients with serious comorbidities such as organ failure or immune diseases. Both the ImmPort database (https://www.immport.org/home/) and the InnateDB database (https://www.innatedb.ca/) were accessed to obtain a list of immune-related genes. The TCGA tumor samples were separated into 6 different immune subtypes after being classified according to the 5 immune expression features [13].

First, we used differential analysis and weighted gene co-expression network analysis (WGCNA) to search for hub IRGs that are associated with LUAD. This allowed us to narrow down the number of potential candidate genes. In the next step, we used univariate and multivariate Cox proportional hazards models to create and analyze the prognostic model for IRGPI. The tumor samples were divided into high-risk and low-risk subgroups using the median IRGPI as the threshold, and the molecular and immunological characteristics of the two categories were examined. Finally, we modeled the effectiveness of immune checkpoint inhibitors by employing CTLA4 expression, TMB, and tumor immune dysfunction and exclusion (TIDE).

Selection of immune-related hub genes

The genes in the LUAD samples obtained from TCGA were evaluated for differential expression using the Limma package, and the differentially expressed genes (DEGs, logFC>1 and FDR<0.05) were then retrieved. The acquired DEGs were intersected with the list of immune-related genes (IRGs), and the DEGs were analyzed by means of GO and KEGG enrichment analyses using the ClusterProfiler package.

The WGCNA package was used to perform the co-expression analysis of the DEGs. Then, the most effective soft-threshold ($\beta = 4$) was received with the aid of univariate linear regression. According to the appropriate soft-threshold, the degree of correlation that exists between two genes was determined. Finally, the minimum number of genes that must be present in each module was set to 25 so that clustering could be performed successfully. We constructed a full set of 4 modules, and we

obtained the connection between each module and clinical characteristics. The light green module had the largest *p*-value, and a co-expression network was constructed.

An analysis of 270 genes in the light green module using univariate Cox regression revealed that the overall survival of LUAD patients and 55 hub genes were statistically significantly correlated (P<0.05). With the survminer package, a calculation was made to determine the optimal cutoff value for each gene's expression. The patients were divided into two clusters, one with low expression and one with high expression, depending on the cutoff value. The Kaplan-Meier (K-M) technique was used to draw survival curves, and the corresponding *p*-values were obtained. The Maftools package was used to perform the calculation, after which the mutation data of 55 immune-related prognostic genes in these LUAD patients were analyzed.

Construction of lung adenocarcinoma immune-related gene prognostic index (IRGPI) model

A multivariate Cox regression analysis was performed on the 55 genes that were found. 16 genes had a significant relationships with prognosis. The Cox proportional hazards model known as IRGPI is generated by multiplying the expression levels of a group of genes with the assistance of coefficients that are associated with those levels. The K-M approach was used to conduct a survival study on the TCGA and GEO cohorts to validate the utility of the IRGPI in determining the likely outcome of treatment for LUAD patients. Finally, univariate and multivariate Cox regression analyses of the IRGPI and common clinical prognostic indicators were carried out with the intention of conducting further testing of the independent prognostic capacity of the IRGPI. In this study, clinical prognostic indicators such as gender, age, TNM stage, and clinical stage were taken into account.

Gene set enrichment analysis (GSEA) and tumor mutational burden (TMB)

First, we employed the Limma package for differential expression evaluation of the clusters to attain their DEGs to create the various signaling pathways that are characteristic of the two clusters. Subsequently, the GO and KEGG gene units were retrieved from the MSigDB database (http://www.gsea-msigdb.org/), and we carried out GSEA enrichment analysis using the ClusterProfiler package. The Maftools program was then used to conduct an analysis of the single nucleotide mutation statistics of LUAD patients. This was done to obtain the gene mutation facts of these two clusters. To investigate the variations in CTLA4 expression and TMB that exist between the two groups, the Limma package was used.

Tumor microenvironment (TME)

Twenty-two distinct immune cells were evaluated for invasion using the CIBERSORT algorithm. The IRGPI TME landscape was obtained using this information. After that, we analyzed the percentages of 22 distinct immune cells between the two IRGPI clusters by using the Limma package, and we showed the K-M survival curves to identify which cells had an impact on prognosis.

Clinical correlation analysis

The chi-square test was used to investigate the spread of immunologic subtypes and clinical phases among the two clusters. The goal of this investigation was to obtain an understanding of the link between immunity and clinical categorization technique.

Prognostic capacity and immunotherapy response of IRGPI

We determined the TIDE score of the TCGA samples to forecast the effectiveness of immunotherapy as a treatment in various IRGPI subgroups (http://tide.dfci.harvard.edu/). The area under the curve (AUC) for the variables IRGPI, TIDE, and tumor inflammatory features (TIS) was calculated using the timeROC package. This was carried out to verify the dependability of IRGPI as a predictive biomarker. Evidence for IRGPI as an excellent model was obtained.

Statistical analysis

R software (version 4.1.2) and associated R packages were used in the generation of each graph and statistical analysis. We carried out enrichment analyses for GO, KEGG, and GSEA

using the ClusterProfiler package. The timeROC software package was used in the calculation of the ROC curves and the AUCs. Chi-square analysis was used to determine whether the differences between the two IRGPI categories were significant. The variables connected to prognosis were identified using a Cox regression model. A *p*-value <0.05 was considered significant.

Results

Immune-related hub genes in LUAD

Between the 59 normal samples and the 539 tumor samples, 8,275 DEGs were recorded in total. They showed a down-regulation of 1,812 genes and an up-regulation of 6,463 genes (**Figure 1A**). We performed a genome-wide search for immune genes using InnateDB and ImmPort and compared them to the DEGs that were generated. In total, 678 immune-related DEGs were identified, with 429 showing up-regulation and 249 showing down-regulation (**Figure 1B**). GSEA analysis of the DEGs revealed that 678 of them were significantly linked to 1,754 GO keywords and 67 KEGG pathways. The top 8 GO elements and KEGG pathways are shown in **Figure 1C** and **1D**. There were several different immune responses enriched in DEGs. We discovered that DEGs could mediate the body's immunologic response and complement activation based on the above analysis. Several of the DEGs were abundant in cytokine signaling, chemokine signaling, and complement pathways, according to KEGG pathway analysis. As a result, we concluded that the examined genes are linked to immunity.

We utilized WGCNA to find hub genes from immune-related DEGs. First, using a 20,000-sample upper limit, we identified outliers in the cluster and removed 1 sample. The optimal soft threshold was discovered to be 4 (**Figure 2A**). 4 modules in total, including the gray module, were produced (**Figure 2B**, **2C**). We selected the light green module, which was most strongly associated with LUAD for analysis based on the *p*-value. The light green module has 270 genes. The co-expression network of the light green module showed 19 genes and 24 edges when we adjusted the threshold weight to be larger than 0.30 among them (**Figure 2D**). The 270 genes found in the light green module were analyzed using univariate Cox regression, and the results showed that 55 hub IRGs were significantly connected with the prognosis of LUAD patients (**Figure 4A**). After that, a K-M survival analysis was performed to validate the prognostic significance of the hub genes, and survival curves were shown for the 12 genes that had the highest and lowest levels of prognostic risk (**Figure 3**).

We then analyzed the mutation profiles of the 55 key IRGs. Missense mutations were present in most genes, whereas some exhibited nonsense mutations, multiple hits, or splice site mutations (**Figure 4B**). PRKDC, C7, and SEMA3A all had mutation rates that were higher than 4%.

Equation and subgroup analysis of the IRGPI

We carried out a multivariate Cox regression analysis on the 55 IRGs to locate genes with independent prognostic value. Sixteen genes were strongly connected to prognosis (DUOX1, IL7R, PTX3, BIRC5, AGER, PDGFB, ANGPTL4, TNFRSF11A, SHC3, OAS3, CFTR, HSPD1, PLK1, C7, C6, and PRKCE). Then, we built a model based on the prognostic indices of these IRGs using the Cox proportional hazards model. The formula is as follows: DUOX1 * 0.14 + IL7R * (-0.30) + PTX3 * 0.34 + BIRC5 * (-0.29) + AGER * (-0.11) + PDGFB * 0.29 + ANGPTL4 * 0.14 + TNFRSF11A * 0.32 + SHC3 * (-0.18) + OAS3 * 0.19 + CFTR * (-0.15) + HS PD1 * 0.28 + PLK1 * 0.30 + C7 * 0.15 + C6 * (-0.22) + PRKCE * (-0.59).

According to a univariate Cox regression study, IRGPI, clinical stage, and TNM stage were all significantly connected with patient prognosis (**Figure 5A**, **5B**). Multivariate Cox regression analysis further confirmed the above conclusions. Thus, we concluded that the IRGPI is an independent prognostic factor. Next, we calculated the IRGPI for LUAD samples and used the median value as the cutoff level to divide them into high-risk and low-risk subgroups. The low-risk group had higher rates of overall survival across the board in both datasets (P<0.01, **Figure 5C**, **5D**).

Molecular characteristics of the IRGPI clusters

The pathways enriched in each of the two IRGPI subgroups were first determined using GSEA on the two subgroups. The cell cycle, DNA replication, oocyte meiosis, proteasome, and spli-

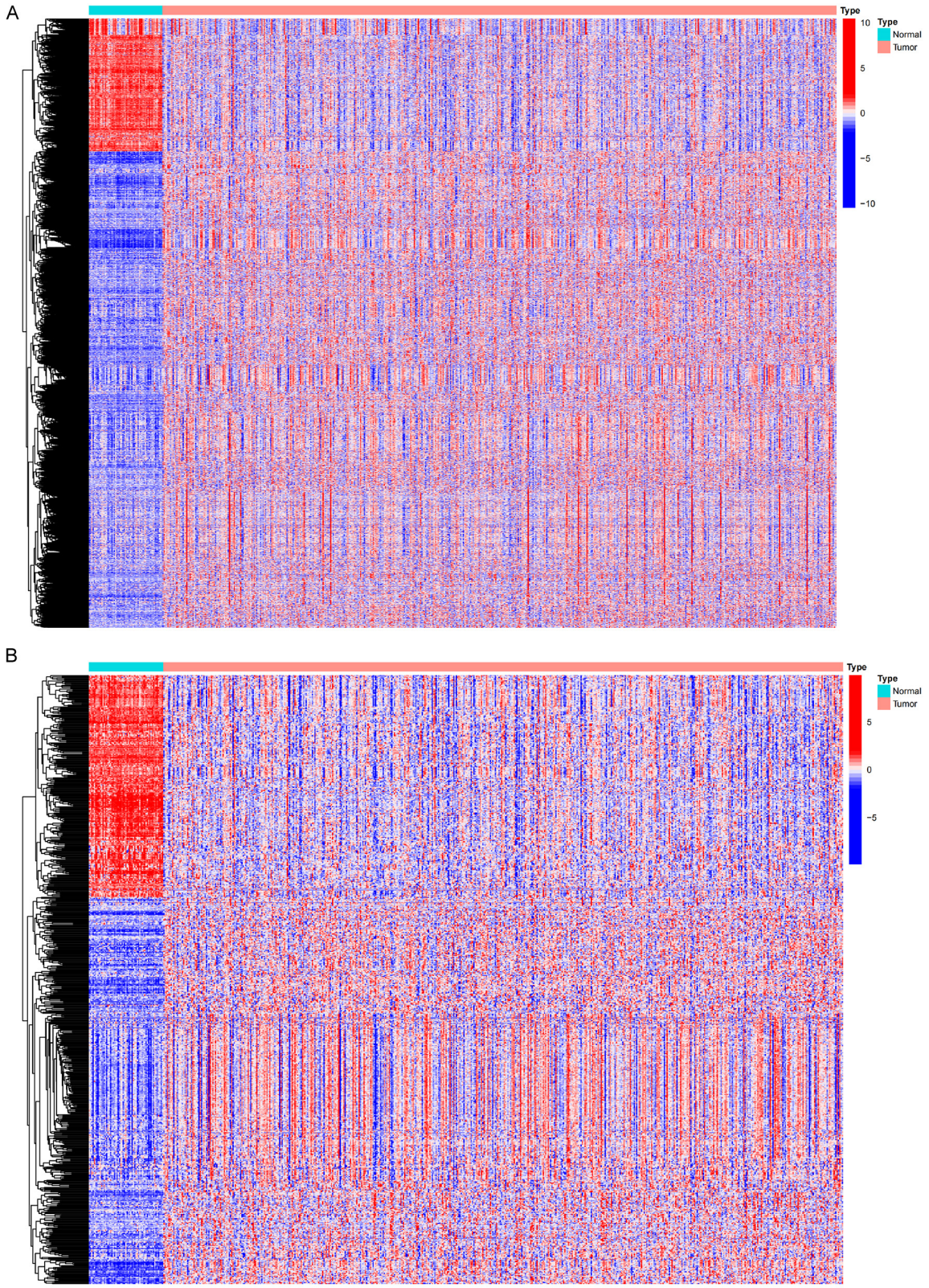
A
Type
Type
Normal
Tumor
10
5
0
−5
−10
B
Type
Type
Normal
Tumor
5
0
−5

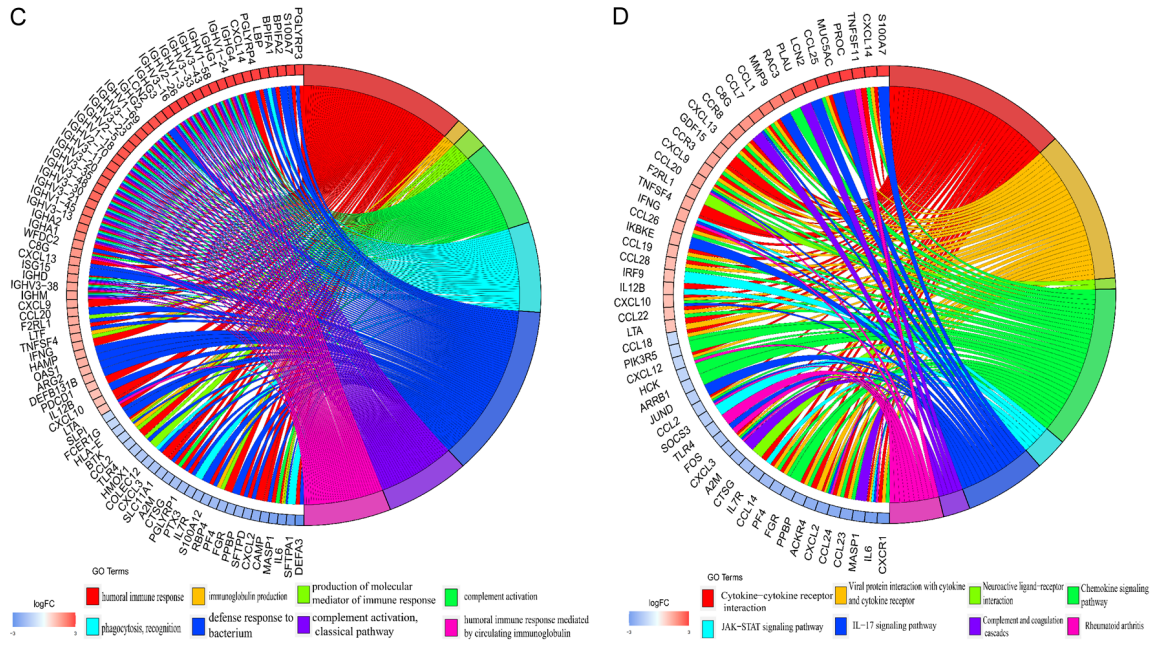

Figure 1. Differential expression analysis in LUAD patients. A. Heat map showing all DEGs between 539 tumor samples (red) and 59 normal samples (blue). B. Heat map showing 678 immune-related DEGs between 539 tumor samples (red) and 59 normal samples (blue). C. GO enrichment analysis of IRGs. D. KEGG pathway analysis of IRGs.

ceosome were primarily enriched in the high-risk group (**Figure 6A**), suggesting that these pathways may be linked to the formation and progression of tumors. Allograft rejection, the hematopoietic stem-cell system, the gut immune network for IgA production, and systemic lupus erythematosus were the major pathways enriched in the low-risk group (**Figure 6B**). The low-risk group had more immune-related gene sets, indicating a stronger immunological microenvironment.

Next, we analyzed the mutated genes in the two subgroups. We identified the 20 most frequently mutated genes and then analyzed the mutation data of the two subgroups, revealing the prevalence of mutations in both subgroups (**Figure 6C**, **6D**). In all groups, we discovered that missense gene mutations were more prevalent than multiple mutations. Among the two groups, the mutation rates for KRAS, USH2A, ZFHX4, LRP1B, RYR2, CSMD3, MUC16, TTN, and TP53 were all greater than 20%. The high-risk group had significantly higher frequencies of TP53 and TTN mutations in comparison to the low-risk group.

Furthermore, we investigated the impact of immune checkpoint inhibitor therapy by examining the connections between the IRGPI score, CTLA4 expression level, and TMB. The expression of CTLA4 was inversely linked to the IRGPI score (P = 0.0011) and was less present in the low-risk group (P = 0.044) (**Figure 7A**, **7B**). The TMB was, however, much more prevalent in the high-risk group (P = 6.2e-07) (**Figure 7C**). This suggests that ICI therapy may be beneficial for both IRGPI subgroups.

Tumor immune characteristics

We simulated the tumor immune microenvironment by examining the infiltration of 22 immune cell types using the CIBERSORT method (**Figure 8A**). Similarly, we divided the samples into high/low subgroups. Using the Limma package, we compared immune cells in the two subgroups (**Figure 8B**). According to the findings, the low-risk group showed a high distribution of resting memory CD4 T cells, resting dendritic cells, resting mast cells, and resting monocytes, while the high-risk group showed a high distribution of activated memory CD4 T cells and M0 macrophages. A higher proportion of activated memory CD4 T cells and M0 macrophages was associated with a poor prognosis in LUAD patients (P<0.05), and these immune cells were widely distributed in the

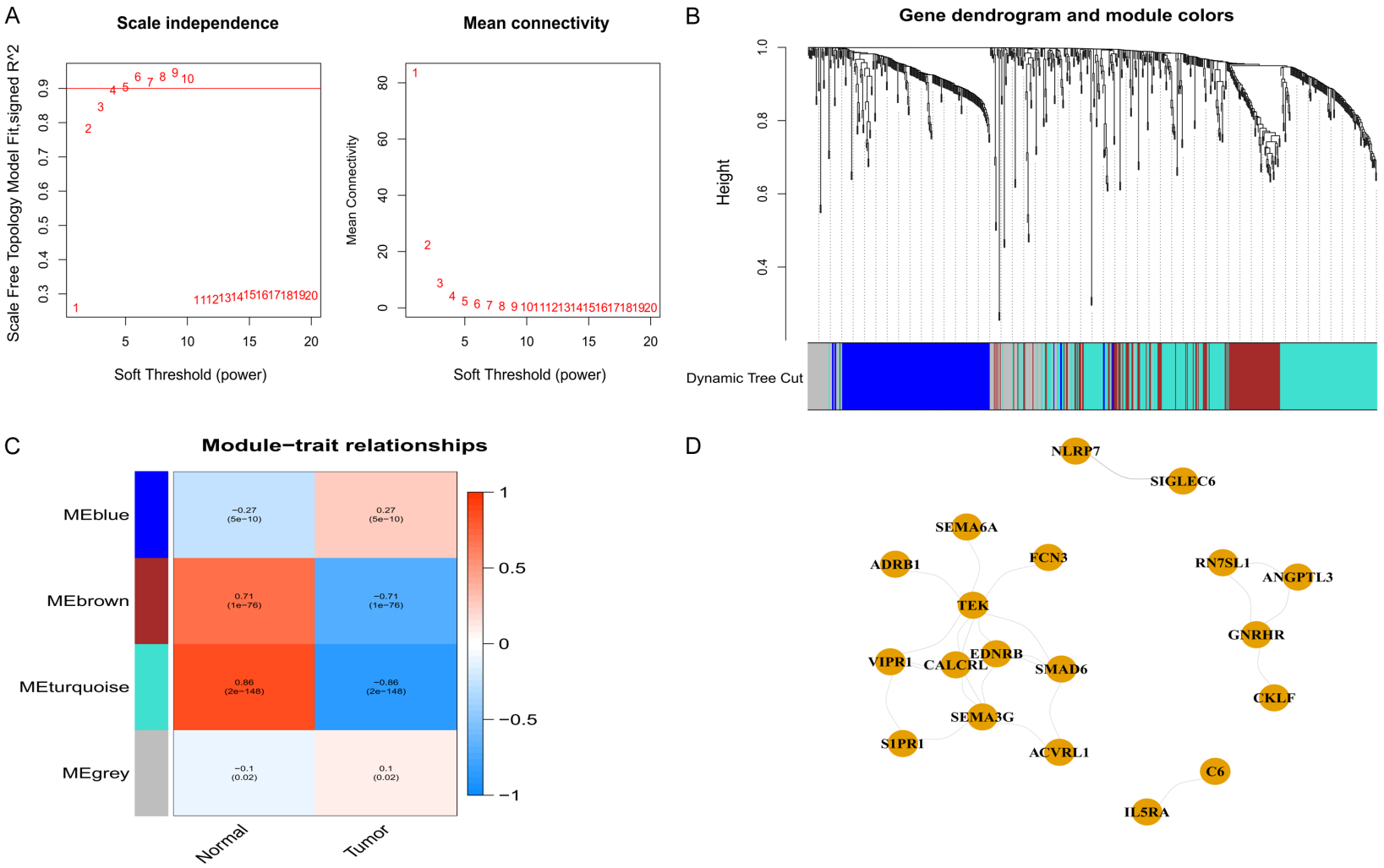

Figure 2. Identification of hub genes in IRGs. A. The horizontal line in the figure indicates a threshold power of 0.90; The optimal soft threshold (power value) was 4. B. Distribution of genes in dendrogram. C. Three non-grey modules were obtained by WGCNA. D. Gene networks in light green modules (threshold weight >0.3).

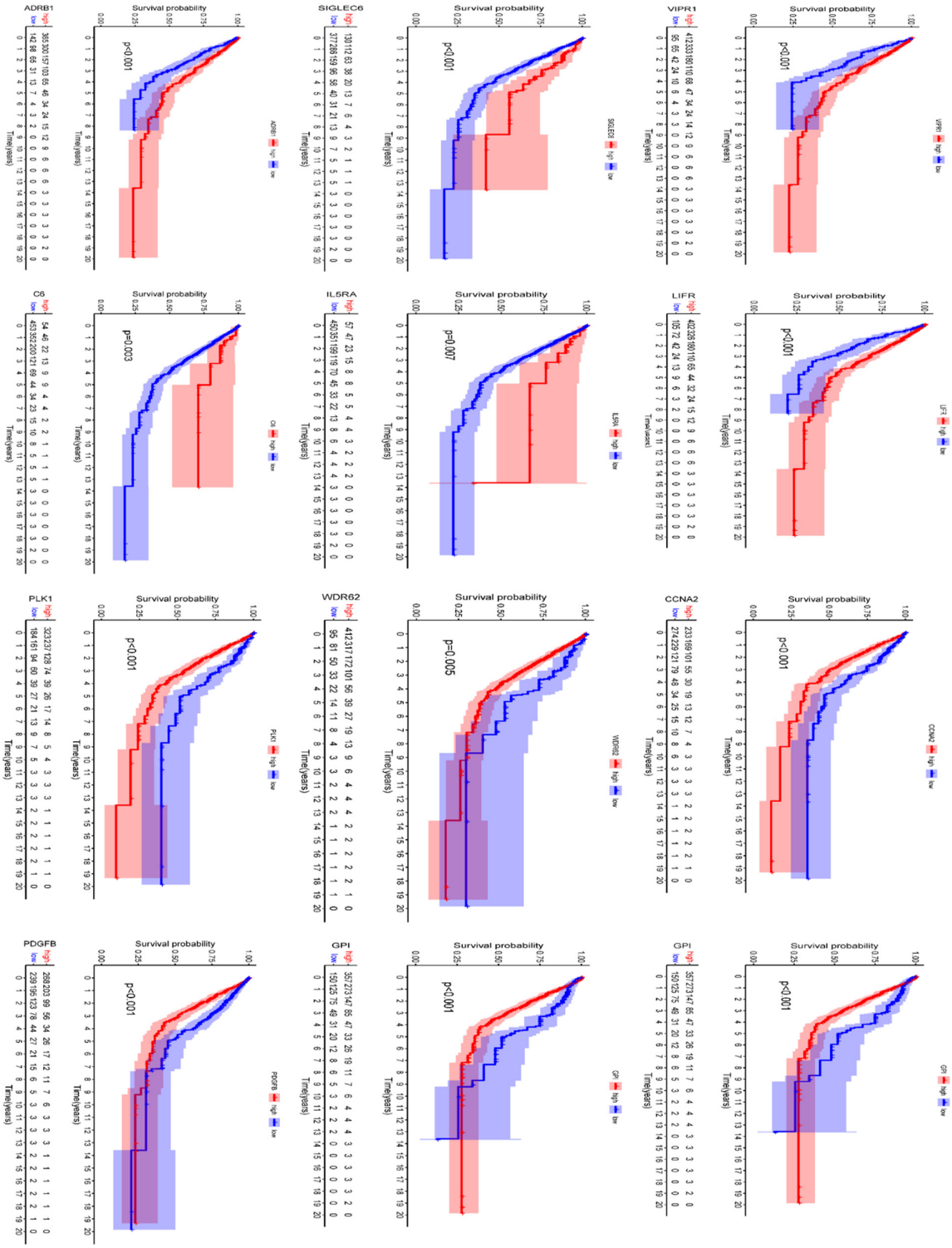

Figure 3. Survival curves for the 12 IRGs with the highest and lowest prognostic risk.

high-risk group. This association was revealed by K-M survival analysis with significant differences in distribution between the two subgroups (**Figure 9**). Because of this, a higher percentage of resting CD4 memory T cells and resting mast cells was linked to a better prog-

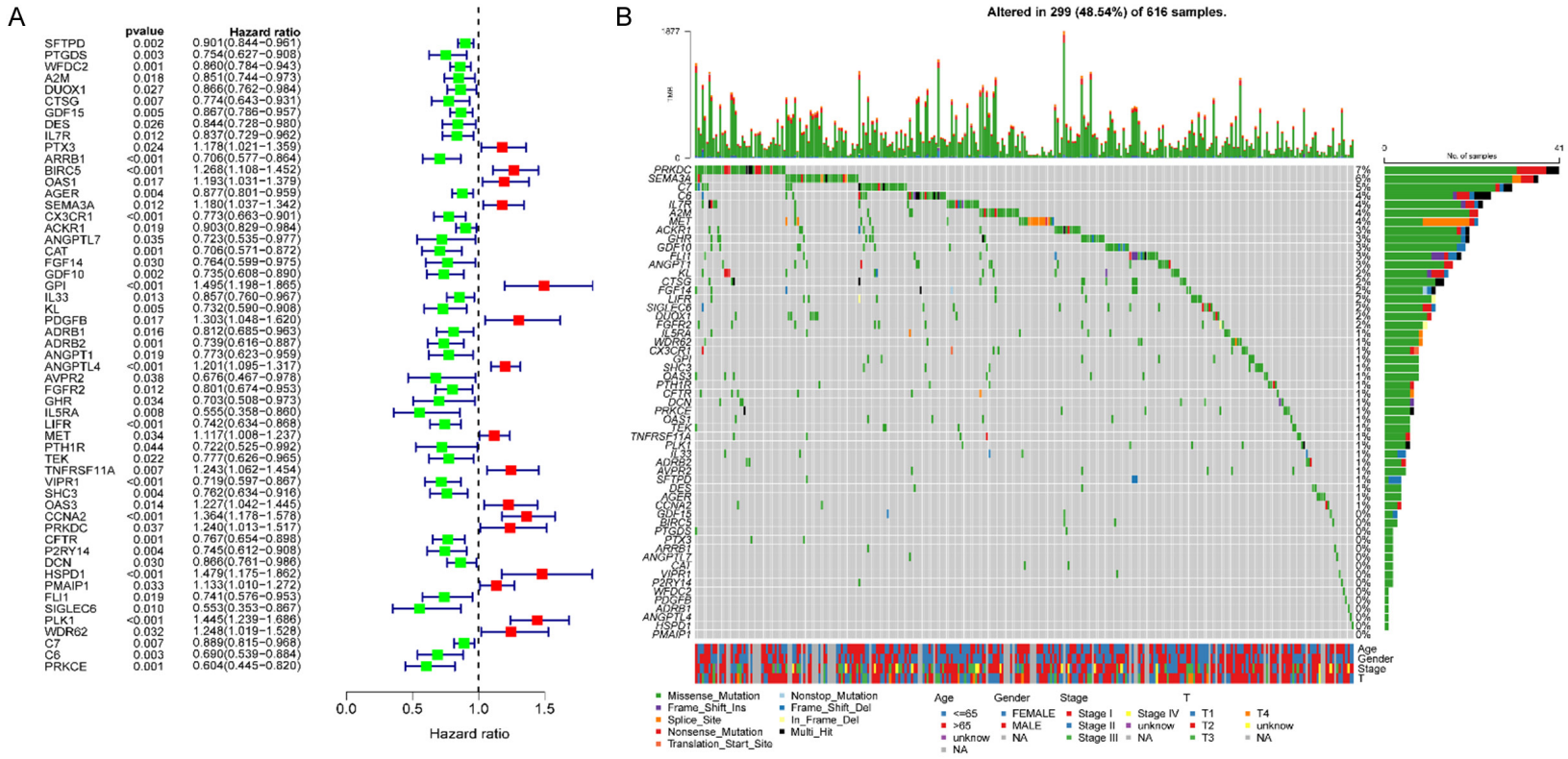

Figure 4. A. Univariate COX analysis of 55 immune-related hub genes (green represents protective factors; yellow represents risk factors). B. Mutations of 55 key IRGs in 539 lung adenocarcinoma samples.

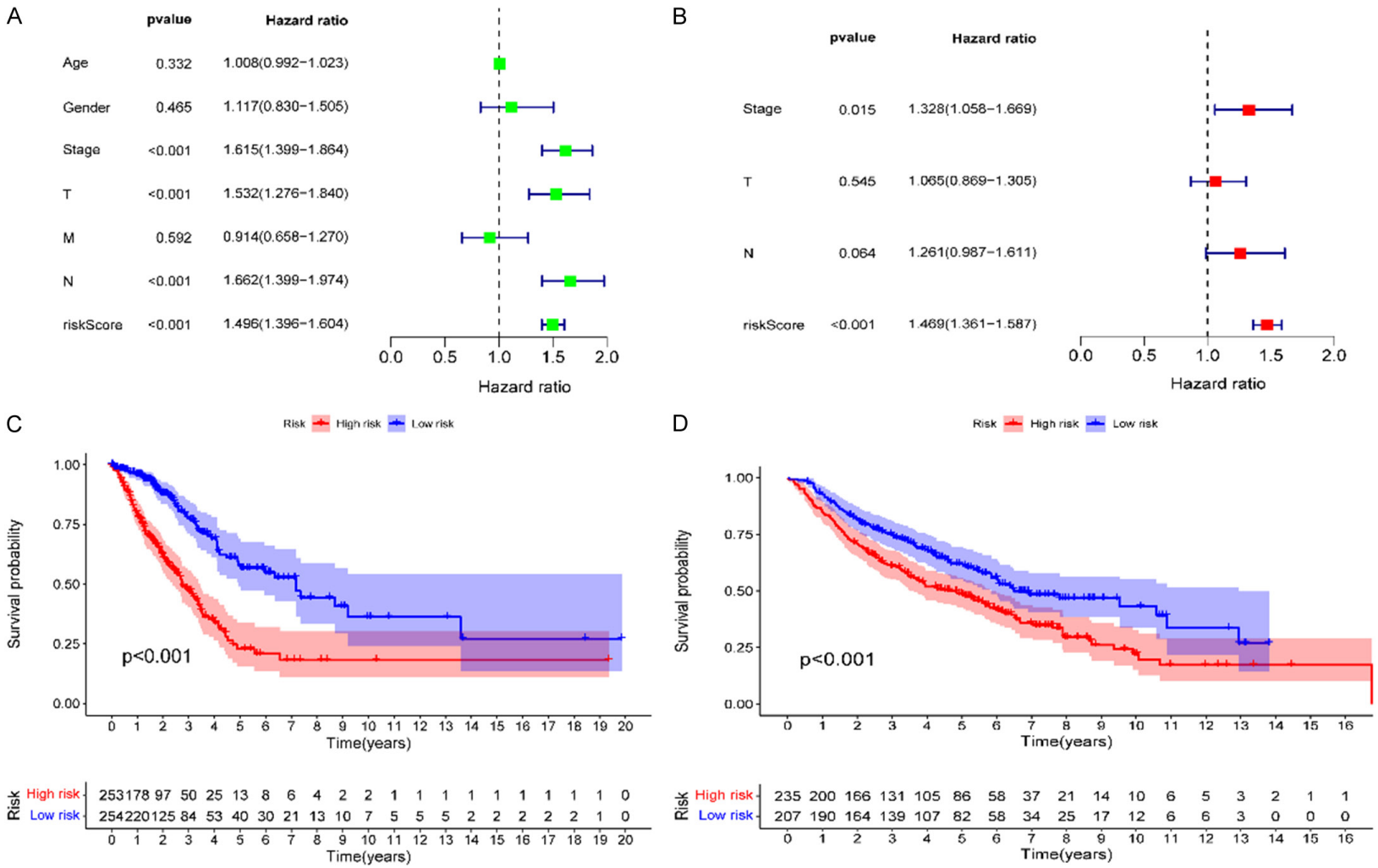

Figure 5. A. Univariate Cox regression analysis showed that IRGPI, clinical Stage (Stage), T stage, and lymph node (N) stage were significantly associated with the prognosis of patients with lung adenocarcinoma. B. Multivariate Cox regression analysis showed that IRGPI and clinical stage were significantly associated with the prognosis of patients with lung adenocarcinoma. C. K-M survival curves of different IRGPI subgroups in TCGA cohort. D. K-M survival curves of different IRGPI subgroups in the GEO (GSE68465) cohort.

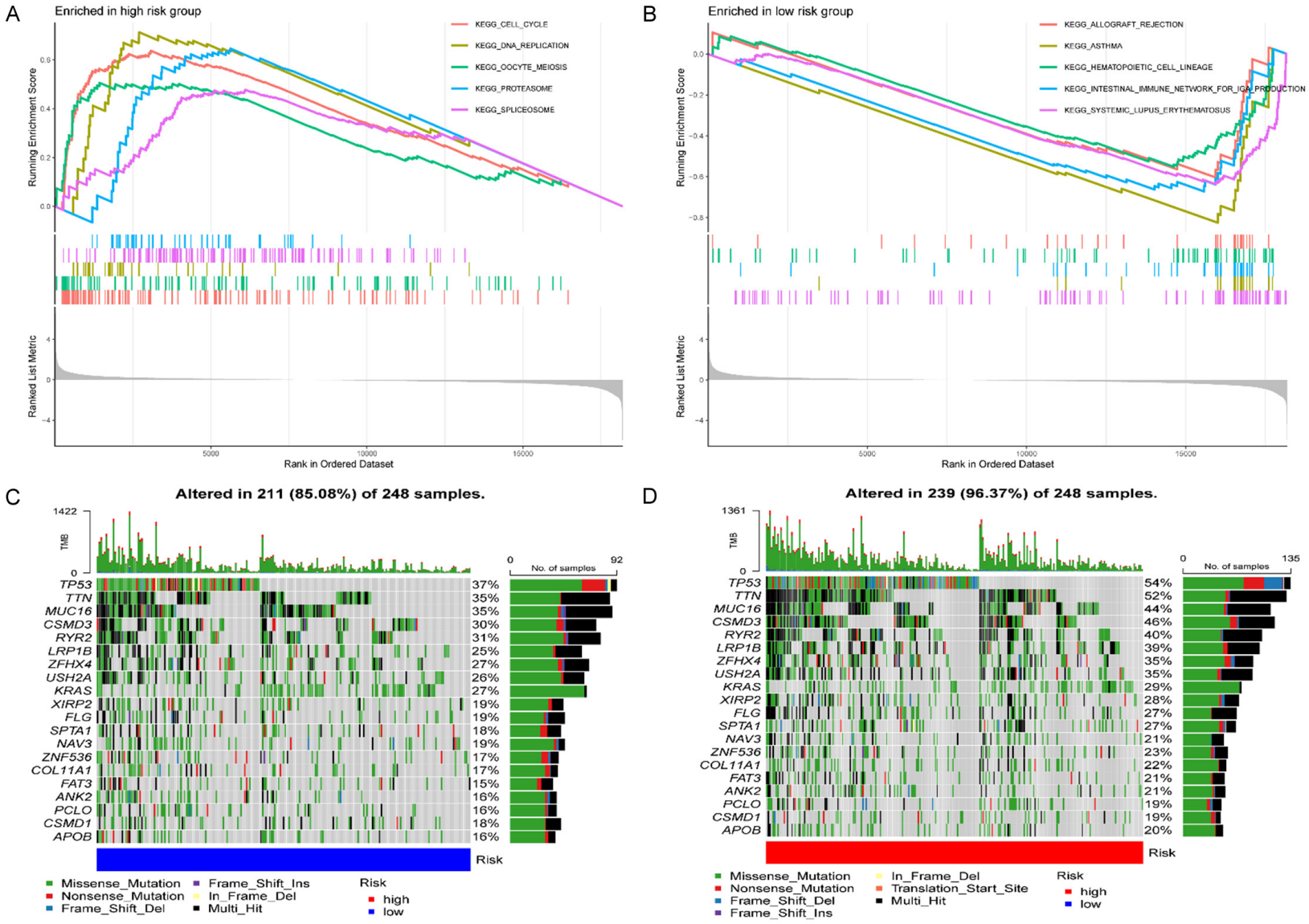

Figure 6. Molecular characteristics of the 2 IRGPI subgroups. A. Main enriched gene sets in IRGPI low-risk group. B. Main enriched gene sets in the IRGPI high-risk group. C. Waterfall plot showing the mutation status of the IRGPI low risk group. The mutated genes were ordered by the number of mutations in the whole sample, showing the top 20 genes. The color represents the type of mutation. D. Waterfall plot showing the mutation status of the IRGPI high-risk group.

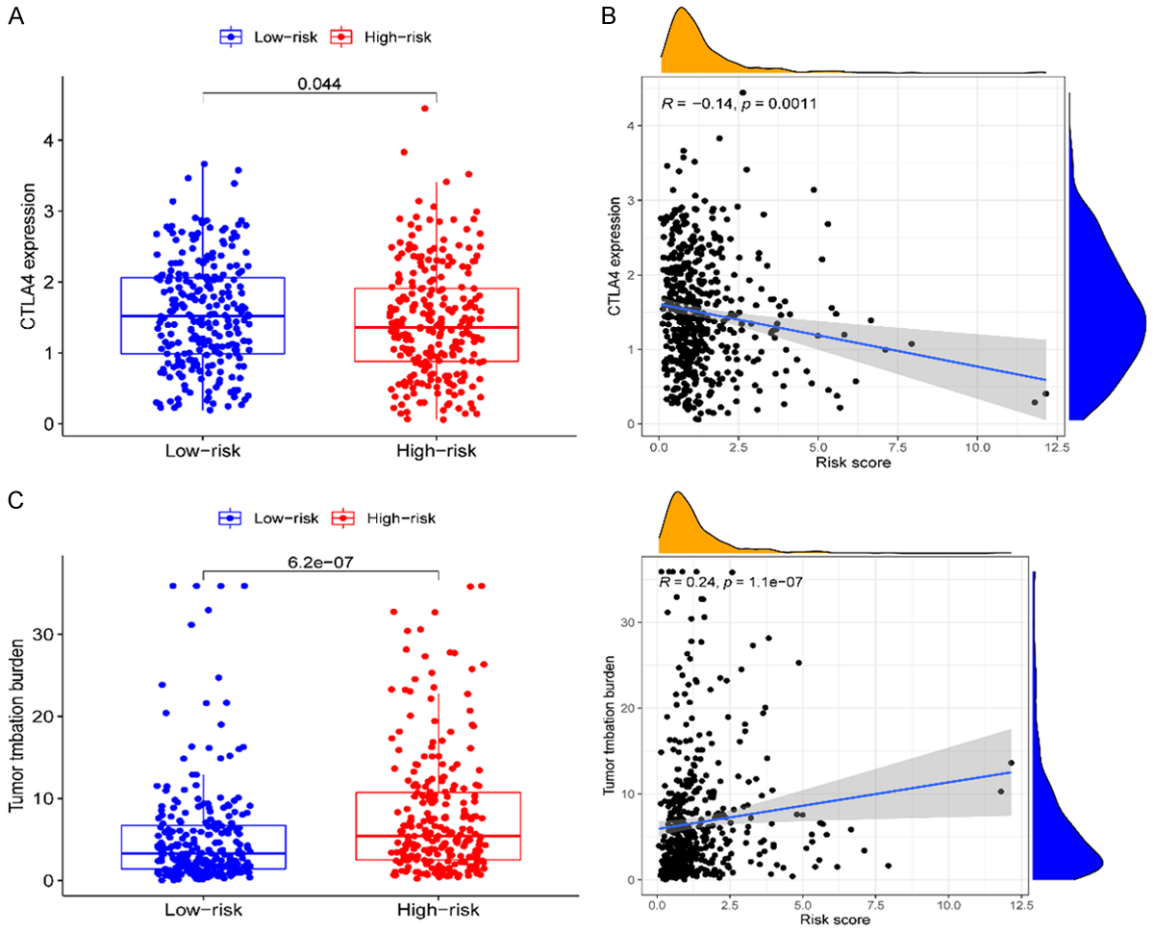

Figure 7. A. Differential expression of CTLA4 between the two subgroups of IRGPI. B. IRGPI score was negatively correlated with CTLA4 expression. C. Differential expression of tumor mutational burden (TMB) between the two subgroups of IRGPI.

nosis in LUAD patients (P<0.01), and these immune cells were prevalent in the low-risk group.

The functional immunological pathways in the high/low-risk groups were then examined. T-cell stimulation, tumor infiltrating lymphocytes (TIL), activated dendritic cells (aDCs), B cells, CD8+ T cells, checkpoint, cytolytic activity, dendritic cells (DCs), human leukocyte antigens (HLA), immature dendritic cells (iDCs), mast cells, neutrophils, T helper cells, and type II IFN response were less significant in the high-risk group (**Figure 8C**). However, there was a strong relationship between this group and major histocompatibility complex (MHC) class I molecules. Following survival analyses (**Figure 10**), high abundances of aDCs, B cells, CD8+ T cells, checkpoints, cytolytic activity, DCs, HLA, iDCs, mast cells, T helper cells, T-cell costimulation, TILs, and type II IFN response were linked to a better prognosis in LUAD patients in addition to increased proportions of MHC class I molecules being significantly connected with a poor prognosis. The prognostic significance of the IRGPI is thus linked to several functional immune pathway enrichments.

Correlation analysis of IRGPI with clinical features, clinical stage, and immune stage

We noticed significant variations in gender, clinical stage (Stage), and TNM stage between the high/low risk IRGPI subgroups (**Figure 11A**). With the highest percentage of stage I patients in both groups, we subsequently examined the difference in clinical stage between them, as shown in **Figure 11B**. However, the proportions of stage II, III, and IV patients in the high-risk group were considerably higher, whereas the

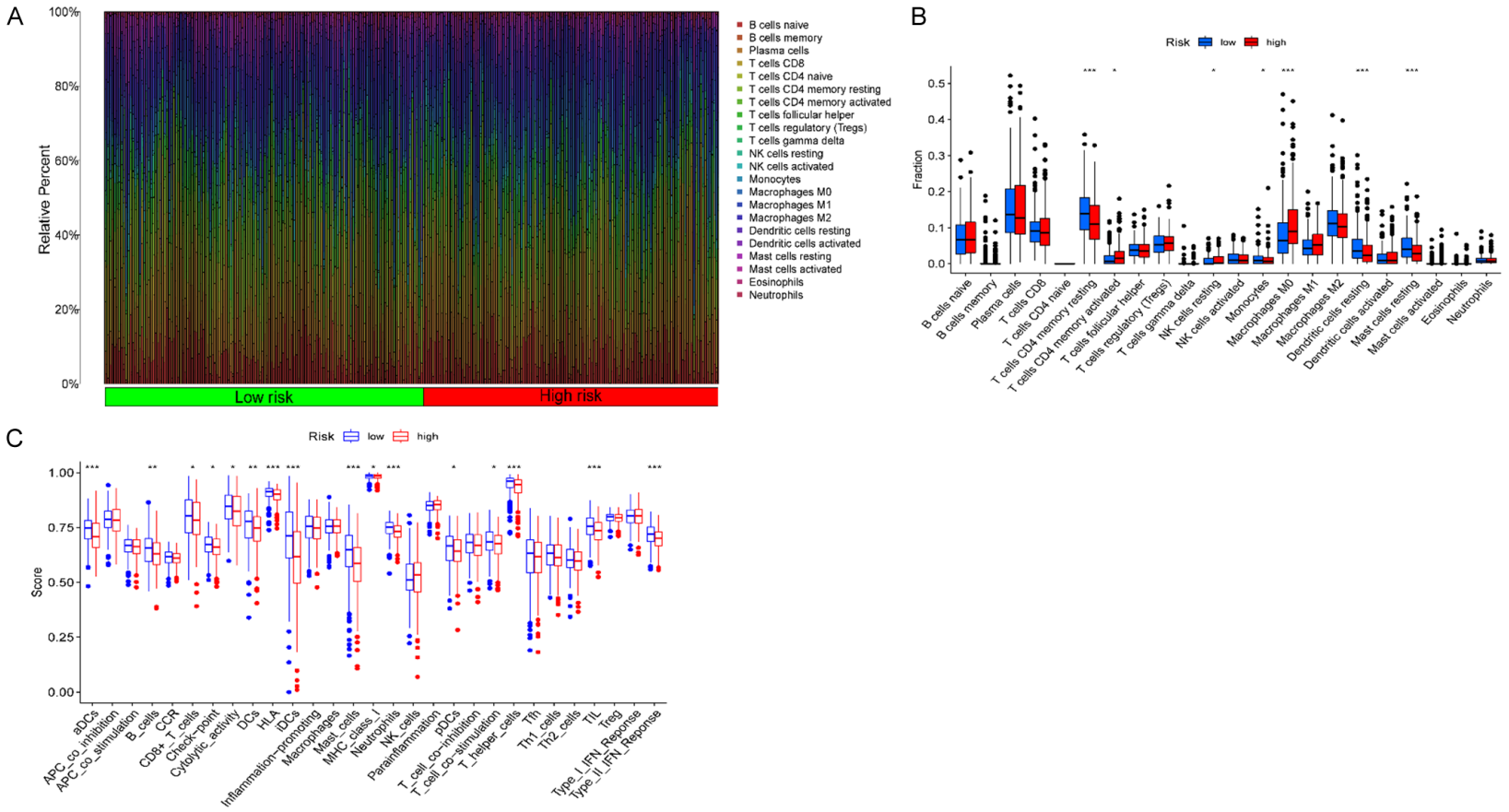

Figure 8. The tumor microenvironment landscape of lung adenocarcinoma patients and the immune characteristics of IRGPI subgroups. A. Relative percentages of 22 immune cells in the TCGA cohort of the 2 IRGPI subgroups. B. Different proportions of tumor microenvironment cells in the two IRGPI subgroups. The scatter points represent the immune cell components of the two IRGPI subgroups. The thick line represents the median value. The bottom and top of the box are 25% and 75%, respectively. "*" indicates that the difference between the two groups is statistically significant (***, P<0.001; **, P<0.01; *, P<0.05). C. There were significant differences in immune-related function scores between the two groups (***, P<0.001; **, P<0.01; *, P<0.05).

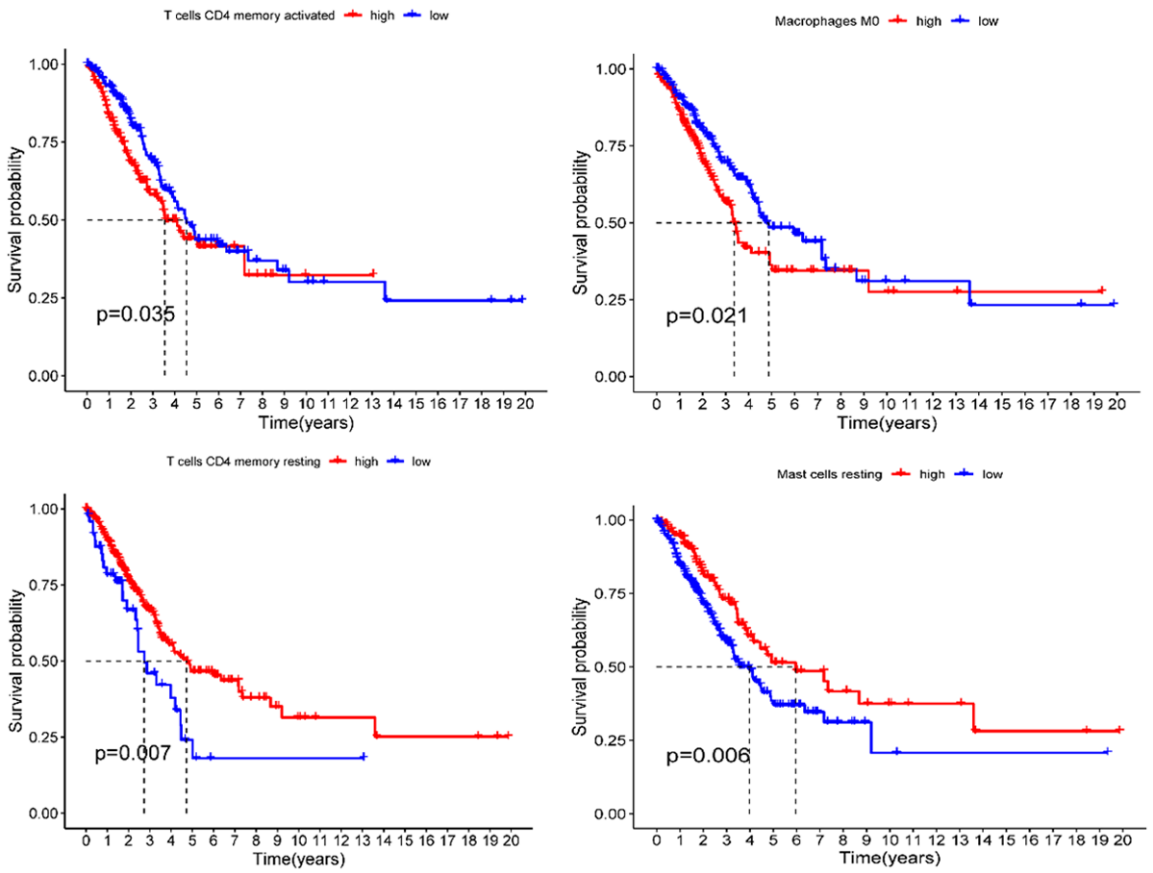

Figure 9. K-M survival curves of immune cells (activated CD4 memory T cells, macrophages, resting CD4 memory T cells, and resting mast cells) were significantly differentially distributed in the two subgroups of IRGPI.

proportion of stage I patients was significantly lower than that in the low-risk group (P = 0.01). Patients in the high-risk group of the IRGPI had a later clinical stage, more severe disease, and a worse prognosis as a result.

Then, based on their immunological features, tumor samples were classified into the C1 (wound healing), C2 (IFN-γ dominated), C3 (inflammation), C4 (lymphocyte depletion), C5 (immune silence), and C6 (TGF-dominated) subtypes. There were appreciable changes in the distribution of immunologic subtypes (**Figure 11C**, P = 0.01). The C1 and C2 made up a higher share of the IRGPI's high-risk subgroup, whereas the C3 made up a larger portion of the IRGPI's low-risk subgroup.

Therapeutic efficacy prediction of immune checkpoint inhibitors (ICIs) and model comparison

TIDE is based on a thorough analysis of the tumor expression profile to predict the efficacy of ICB therapy [14]. We discovered that the T-cell dysfunction scores in the high-risk IRGPI group were lower than those in the other groups (P<0.001), indicating that the low-risk group may have deficient T-cell-mediated immune processes. This finding is depicted in **Figure 12A**. The T-cell rejection scores, however, were greater in high-risk patients (P<0.001), revealing that these tumor cells were better defended from immune attack. Finally, the low-risk group appeared to show a greater ability for immunological escape and to be less susceptible to immunotherapy, as indicated by their higher TIDE scores. It could be concluded that high-risk patients responded better to immunotherapy.

According to the ROC curves, we discovered that the AUC>0.70 at the 1-, 2-, and 3-year (**Figure 12B**). As a result, the IRGPI can be employed as a crucial indicator to forecast patients' prognoses. We discovered that the AUC of the IRGPI was superior to that of the standard TIS and TIDE models, indicating that

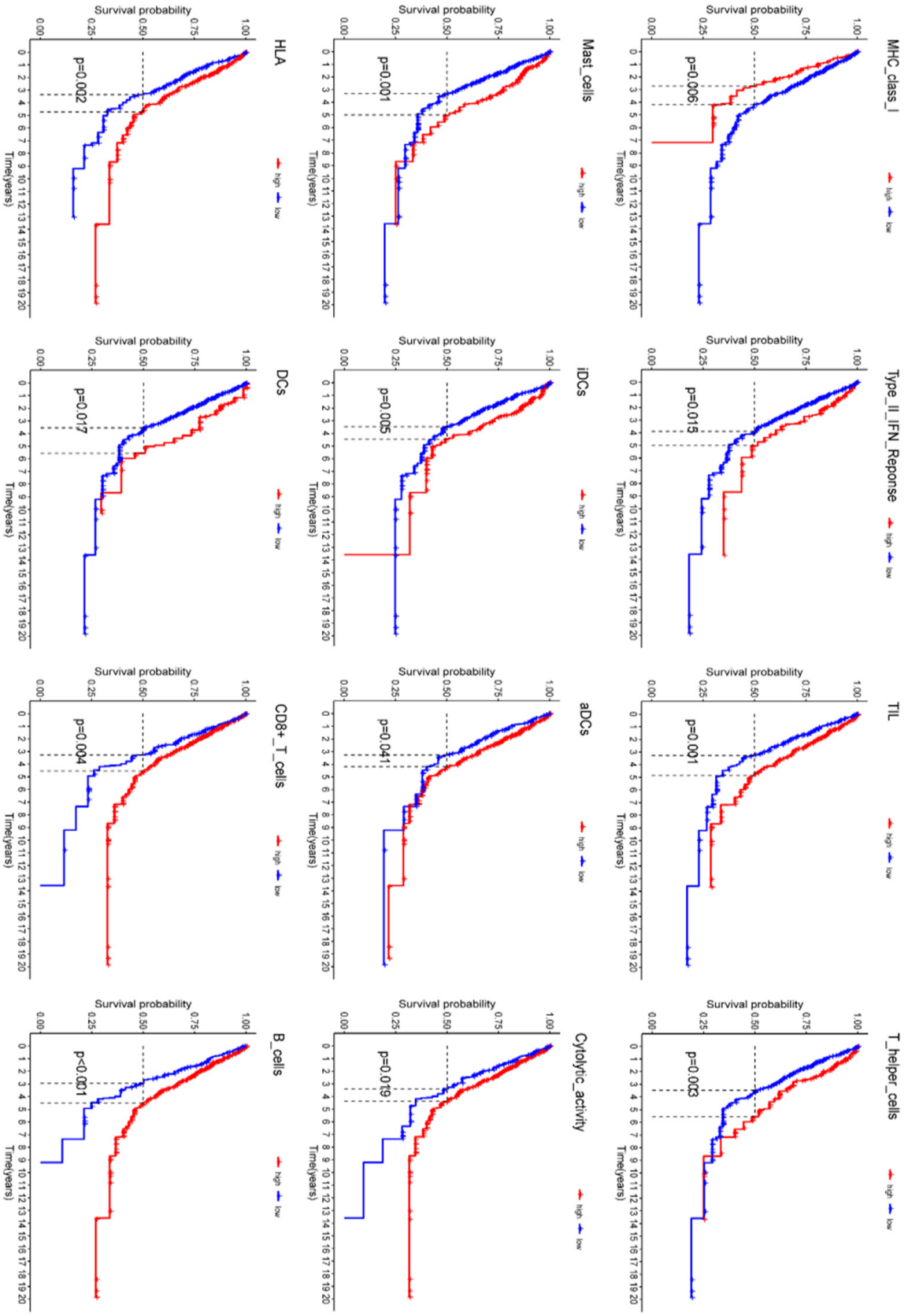
MHC_class_I
p=0.006
Type_II_IFN_Reponse
p=0.015
TIL
p=0.001
T_helper_cells
p=0.003
Mast_cells
p=0.001
iDCs
p=0.005
aDCs
p=0.041
Cytolytic_activity
p=0.019
HLA
p=0.002
DCs
p=0.017
CD8+_T_cells
p=0.004
B_cells
p<0.001
Survival probability
Time(years)
high
low

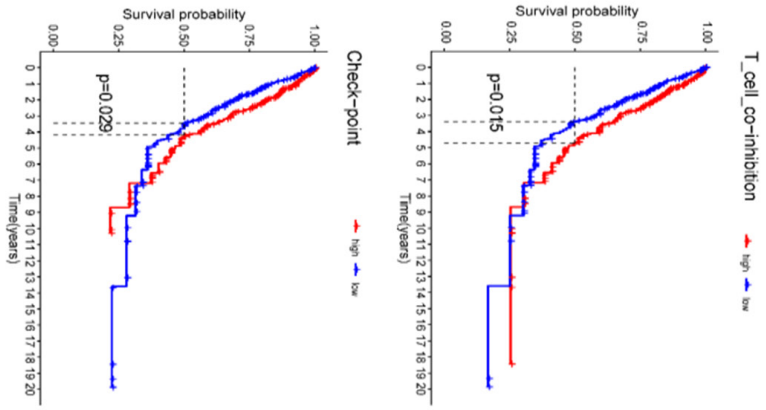

Figure 10. K-M survival curves of immune-related functional pathways were significantly differentially distributed in the two subgroups of IRGPI.

the IRGPI has stronger predictive value than these traditional biomarkers.

Discussion

The prognosis of patients with LUAD and other malignancies can currently be greatly improved by ICIs [12-15]. Immunotherapy's effectiveness does, however, change depending on the patient and the type of malignant tumor [16, 17]. For this reason, investigating which people can benefit from immunotherapy is essential. The prognosis of patients with renal clear cell carcinoma could be predicted by a class of biomarkers based on IRGs, according to previous research [18-20]. There have been few studies on LUAD, and there is no IRGPI model for LUAD that can predict patients' long-term prognoses and the effectiveness of immunotherapy. Thus, a biomarker model based on several IRGs is required to direct therapy strategies.

By using WGCNA and survival analysis, we identified 55 IRGs and built the IRGPI based on 16 genes. People who score high on the IRGPI have a poor prognosis, whereas patients who score low do well. As a result, the IRGPI can be employed as an immune-related biomarker to predict the prognosis of patients with LUAD.

Compared to traditional tumor markers, IRGPI can reflect the prognosis of tumor more comprehensively, from multiple angles and multiple factors. The IRGPI is composed of 16 IRGs: DUOX1, IL7R, PTX3, BIRC5, AGER, PDGFB, ANGPTL4, TNFRSF11A, SHC3, OAS3, CFTR, HSPD1, PLK1, C7, C6 and PRKCE. The protein encoded by ILR7 is the receptor for interleukin-7. High expression of IL-7 and IL7R in LUAD patients is positively correlated with lymph node metastasis and poor survival [21, 22]. IL-7 stimulates the proliferation of tumor cells by upregulating cyclin D1 [23]. In the tumor tissues of patients with lung cancer, there is a positive association between the expression of IL7R and cyclin D1, and the latter is linked to a poor prognosis. The extrinsic suppressor gene PTX3 controls complement dependent, macrophage-persistent, and tumor-promoting inflammation. It is a crucial part of the humoral makeup of innate immunity [24]. The IAP gene family, which includes the BIRC5 gene, produces a negative regulatory protein that prevents apoptotic cell death. To control the interaction between mitosis, apoptosis, and autophagy in cancer cells, the BIRC5 gene can function as a bridging molecule [25]. The advanced glycation end product (AGE) receptor, a cell surface receptor belonging to the immunoglobulin superfamily, is encoded by the AGER gene. The H1299 cells' ability to proliferate, invade, and migrate was inhibited by AGER overexpression, which also increased cell apoptosis [26]. The PDGFB gene encodes a member of the platelet-derived growth factor (PDGF) and vascular endothelial growth factor (VEGF) protein families. Increased quantities of circulating tumor cells, accelerated hypoxia and epithelial-mesenchymal transition in primary tumors, and increased tumor metastasis are all caused by PDGFB downregulation [27]. Increased collagen homolog 3 (Shc3) expression has been linked to hepatocellular carcinoma invasion and metastasis [28]. OAS3 is involved in the coding of 2', 5'-oligoadenylate synthase (OAS). In terms of the level of immune infiltration, the invasion of immunosuppressive cells is strongly linked to OAS3 expression [29]. Mitochondrial proteins encoded by HSPD1 may act as signal-

A

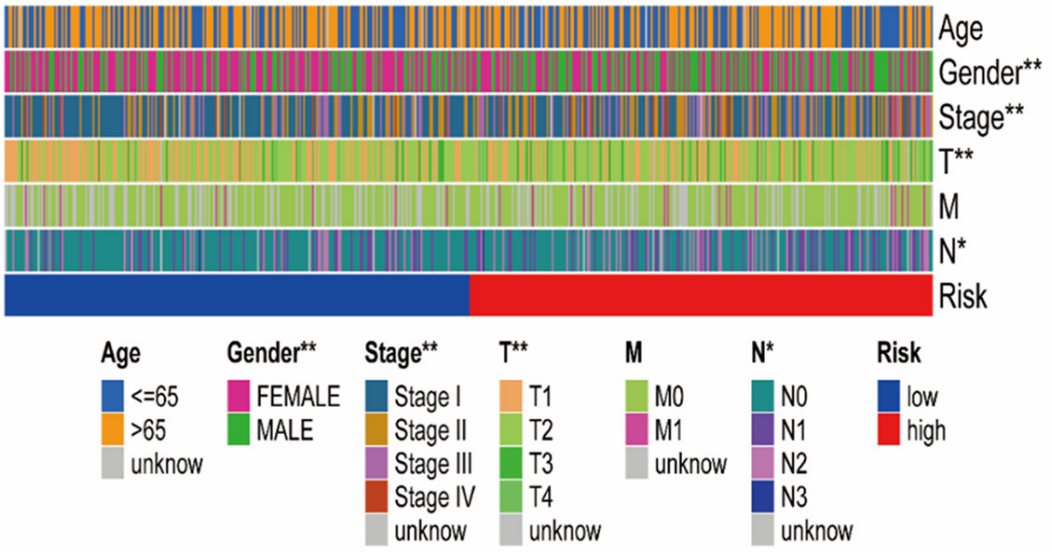

B

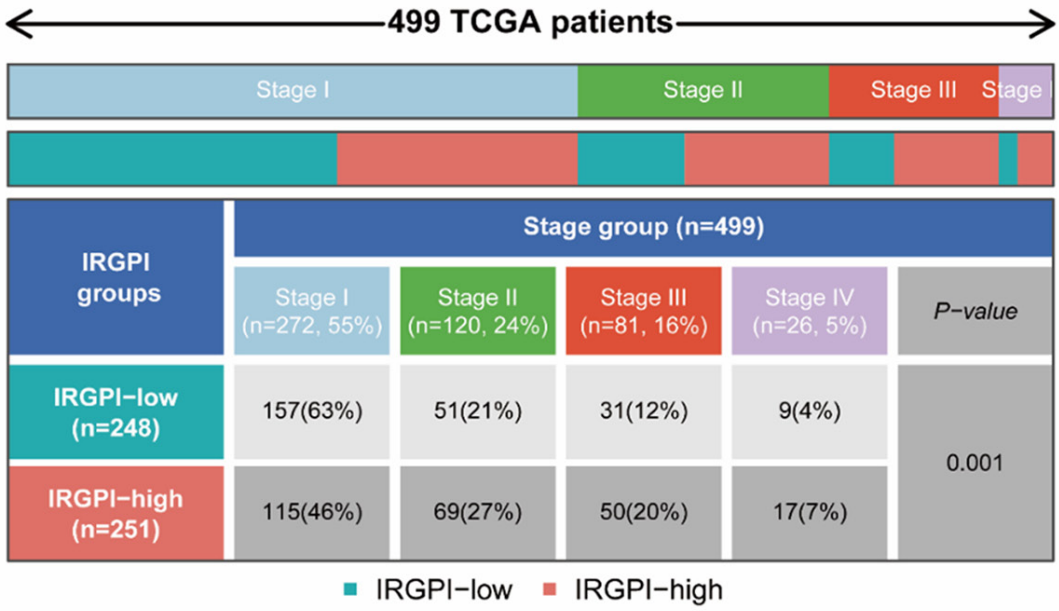

IRGPI groups	Stage group (n=499)				
	Stage I (n=272, 55%)	Stage II (n=120, 24%)	Stage III (n=81, 16%)	Stage IV (n=26, 5%)	*P*-value
IRGPI-low (n=248)	157(63%)	51(21%)	31(12%)	9(4%)	0.001
IRGPI-high (n=251)	115(46%)	69(27%)	50(20%)	17(7%)	

IRGPI-low IRGPI-high

C

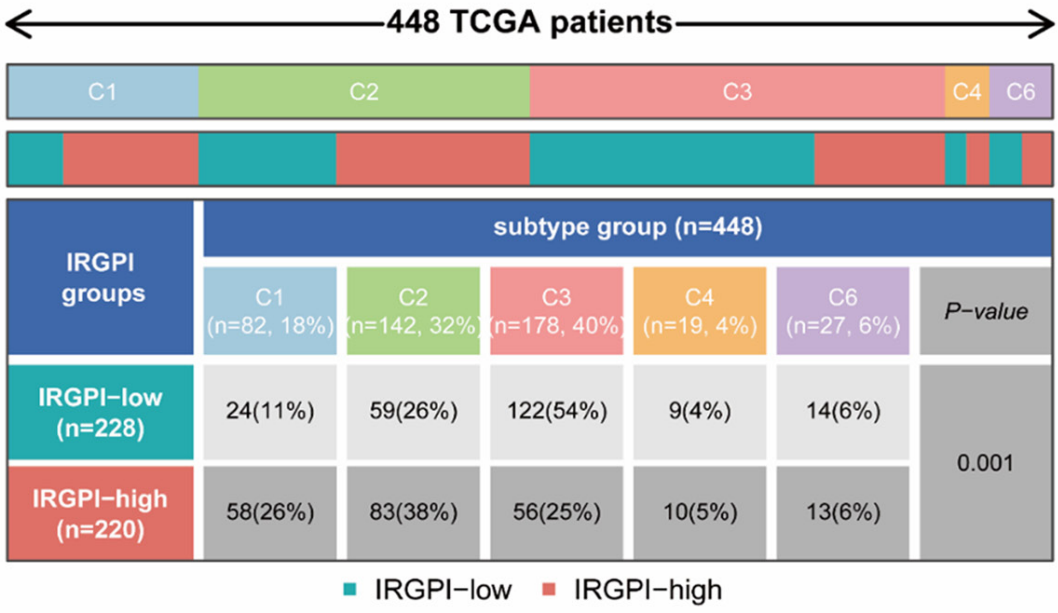

IRGPI groups	subtype group (n=448)					
	C1 (n=82, 18%)	C2 (n=142, 32%)	C3 (n=178, 40%)	C4 (n=19, 4%)	C6 (n=27, 6%)	*P*-value
IRGPI-low (n=228)	24(11%)	59(26%)	122(54%)	9(4%)	14(6%)	0.001
IRGPI-high (n=220)	58(26%)	83(38%)	56(25%)	10(5%)	13(6%)	

IRGPI-low IRGPI-high

Figure 11. A. Analysis of clinical characteristics (age, gender, clinical stage, T, M, N) between the two subgroups (***, P<0.01; *, P<0.05). B. Heat map and table of differential distribution of immunophenotypes (C1, C2, C3, C4, and C6) in lung adenocarcinoma patients between the two IRGPI subgroups. C. Heat map and table of differential distribution of clinical stage (stage I, II, III, IV) in lung adenocarcinoma patients between the two IRGPI subgroups.

ing molecules in the innate immune system and lead to poor prognosis. HSPD1 knockout or destruction can induce a sharp collapse of oxidative phosphorylation and inhibit the proliferation of tumor cells in vitro and in vivo [30]. PLK1 is a key mitotic kinase that is overexpressed and drives cancer growth in various cancers, including NSCLC [31]. C6, C7 are important components of the membrane attack complex as part of the complement pathway of the innate immune system. In conclusion, IRGPI adequately reflects the proliferation, invasion, metastasis, and angiogenesis of lung adenocarcinoma tumor cells and the development of a variety of other tumors.

Somatic mutations are linked to the sensitivity of tumor cells. The response to antineoplastic medications is significantly predicted by these mutations [32]. In the two subgroups, the IRGPI high-risk group had considerably higher TP53 and TTN mutation rates than the IRGPI low-risk group. The acquisition of resistance mutations to EGFR tyrosine kinase inhibitors may be mediated by tumors with TP53 mutations since they have a higher TMB and may work in conjunction with other genomic processes [33]. Furthermore, LUAD patients with TP53 missense mutations responded better to anti-PD-1/L1 immunotherapy than those with nonsense mutations, according to a study that found an association between TP53 missense mutations and elevated PD-L1 levels. Moreover, we discovered that missense mutations dominated TP53 in both groups. Titan-antisense RNA1 (TTN-AS1), a long noncoding RNA (lncRNA) that is produced on the TTN antisense strand, is increased in LUAD and binds to miR-142-5p. It indirectly upregulates the expression of cyclin-dependent kinase 5 as competitive endogenous RNA (ceRNA) (CDK5). The proliferation, invasion, and migration of LUAD cells may all be greatly slowed by TTN-AS1 knockdown [34]. In the IRGPI high-risk category, TP53 and TTN may represent viable targets for immunotherapy and targeted treatment.

TMB is essential for ICI treatment as well as the prognosis. According to our research, the degree of immune cell infiltration between the two clusters differed significantly. The low-risk group had high concentrations of resting dendritic cells, mast cells, and monocytes, which are favorably linked with overall survival and progression-free survival in LUAD patients [35-37]. These cells share the trait of being directly or indirectly involved in the antigen presentation procedure, which enhances prognosis. In the presence of significant infiltration, T cells exhibit antitumor effects and are favorably linked with prognosis. Whereas resting CD4 memory T cells are more prevalent in normal tissues, active immune cells, such as activated CD4 memory T cells, are largely concentrated in tumor tissues [38]. These results are supported by our data, which also show how many different immune cells are present and how active they are in influencing the immunological response and clinical outcome. In future studies, the characteristics of the TMEs of the two IRGPI subgroups should be explored further.

We discovered that a poor prognosis was more likely in those with a high IRGPI. Significant variations in immunologic subtypes existed between the two groups as well. The C1 subtype has a high rate of tumor growth and increased angiogenic gene expression. The C2 subtype has a high incidence of tumor growth and participates in TCR diversity. The C3 subtype has a mild to moderate tumor growth rate and is distinguished by significant Th17 and Th1 cell infiltration, according to some research [13]. C3 has the best prognosis, but C2 and C1 have a poor prognosis despite having significant immunologic components. Moreover, survival studies in the TCGA and GEO cohorts, which aid in the prediction of the immunophenotype profile and the course of the illness in LUAD patients, confirmed this.

CTLA4 protein and TMB are two commonly used biomarkers, both of which are positively correlated with the effect of immunosuppressive therapy [9, 39]. In our investigation, the high-risk group had considerably greater TMB levels and lower CTLA4 expression levels. As a result, we utilized TIDE analysis to forecast how well immunosuppressive medication would

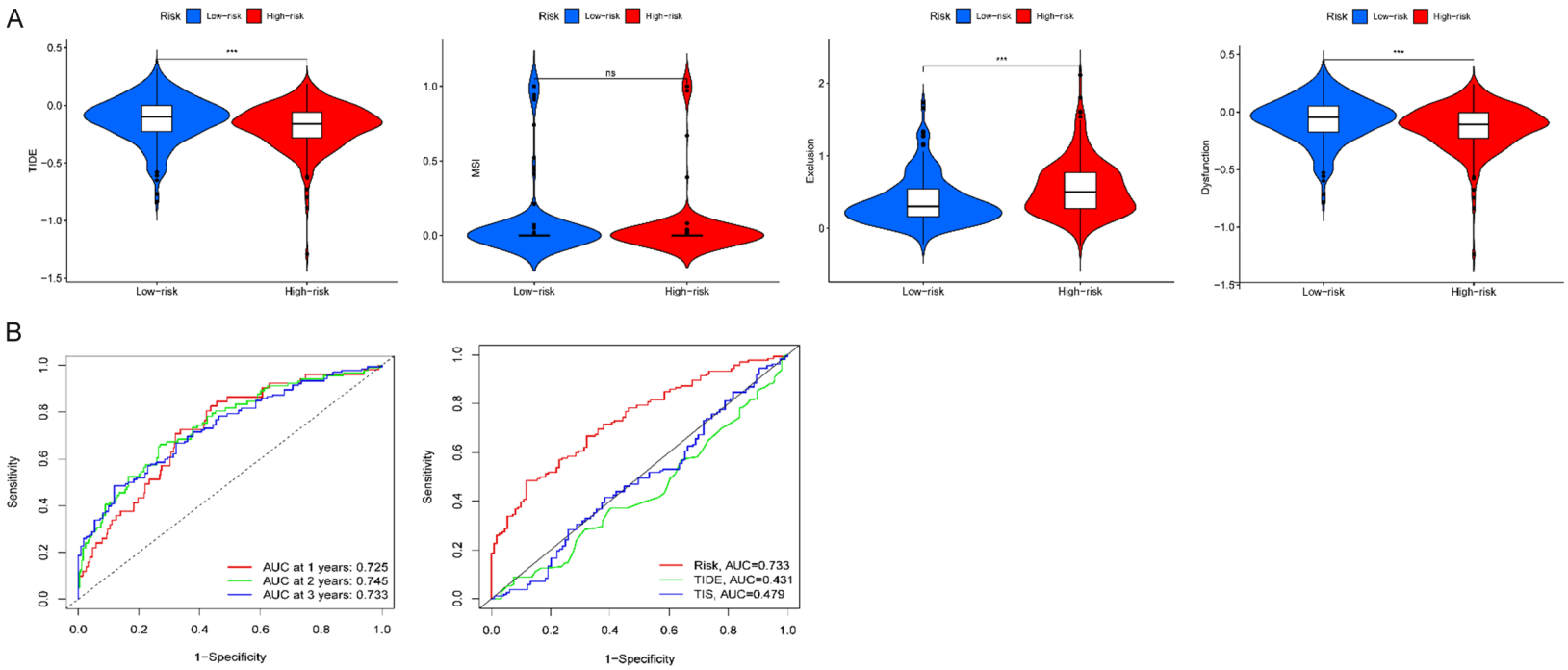

Figure 12. Prognostic value of IRGPI and its response to therapy. A. TEDE, MSI, T cell rejection, and T cell dysfunction scores (ns, no statistical significance; ***, P<0.001). B. Time-dependent ROC analysis of IRGPI, TIS, and TEDER on overall survival at 1, 2, and 3 years of follow-up in the TCGA cohort.

work. The low-risk group had a higher TIDE score than the high-risk group. Therefore, by comprehensive analysis, patients with high-risk of IRGPI had better efficacy of immunotherapy. The IRGPI is a potential biomarker for clinical use since it corrects the standard biomarkers' unbalanced reflection of prognosis. We can thus conclude that the IRGPI model was a more accurate predictive prognostic indicator than the conventional TIS model and TIDE model.

Future therapeutic applications of the IRGPI can offer LUAD patients a wealth of information, including prognosis prediction, a picture of the TME landscape, and the advantage of immunotherapy. This will aid in choosing the best course of treatment. Our follow-up research will focus on the fact that our study needs more real-world study verification and validate the model constructed in this study by immunohistochemistry.

Conclusions

The IRGPI is a promising biomarker for clinical practice that can guide clinical diagnosis and treatment plans. By utilizing important immune-related differential genes, the IRGPI overcomes the drawbacks of conventional biomarkers and lessens the bias of prognostic models, making it a more accurate prognostic indicator. The relevance of this biomarker in enabling customized treatment plans is increased by the ability of the IRGPI to predict how LUAD patients would respond to ICI therapy.

Acknowledgements

This study was supported by Government of Jiangsu Province (BK20191174).

Disclosure of conflict of interest

None.

Address correspondence to: Dr. Hai-Tao Ma, Department of Thoracic Surgery, Suzhou Dushu Lake Hospital (Dushu Lake Hospital Affiliated to Soochow University, Medical Center of Soochow University), Soochow University, No. 9 Chongwen Road, Suzhou 215000, Jiangsu, China. E-mail: mht74003@163.com; Dr. Wei Song, Emergency Department, Suzhou Dushu Lake Hospital (Dushu Lake Hospital Affiliated to Soochow University, Medical Center of Soochow University), Soochow University, No. 9 Chongwen Road, Suzhou 215000, Jiangsu, China. E-mail: hini1983@163.com

References

[1] Chen J, Yang H, Teo ASM, Amer LB, Sherbaf FG, Tan CQ, Alvarez JJS, Lu B, Lim JQ, Takano A, Nahar R, Lee YY, Phua CZJ, Chua KP, Suteja L, Chen PJ, Chang MM, Koh TPT, Ong BH, Anantham D, Hsu AAL, Gogna A, Too CW, Aung ZW, Lee YF, Wang L, Lim TKH, Wilm A, Choi PS, Ng PY, Toh CK, Lim WT, Ma S, Lim B, Liu J, Tam WL, Skanderup AJ, Yeong JPS, Tan EH, Creasy CL, Tan DSW, Hillmer AM and Zhai W. Genomic landscape of lung adenocarcinoma in East Asians. Nat Genet 2020; 52: 177-86.

[2] Ettinger DS, Wood DE, Aisner DL, Akerley W, Bauman JR, Bharat A, Bruno DS, Chang JY, Chirieac LR, D'Amico TA, DeCamp M, Dilling TJ, Dowell J, Gettinger S, Grotz TE, Gubens MA, Hegde A, Lackner RP, Lanuti M, Lin J, Loo BW, Lovly CM, Maldonado F, Massarelli E, Morgensztern D, Ng T, Otterson GA, Pacheco JM, Patel SP, Riely GJ, Riess J, Schild SE, Shapiro TA, Singh AP, Stevenson J, Tam A, Tanvetyanon T, Yanagawa J, Yang SC, Yau E, Gregory K and Hughes M. Non-small cell lung cancer, version 3.2022, NCCN clinical practice guidelines in oncology. J Natl Compr Canc Netw 2022; 20: 497-530.

[3] Simoff MJ, Lally B, Slade MG, Goldberg WG, Lee P, Michaud GC, Wahidi MM and Chawla M. Symptom management in patients with lung cancer: diagnosis and management of lung cancer, 3rd ed: American College of Chest Physicians evidence-based clinical practice guidelines. Chest 2013; 143 Suppl: e455S-e497S.

[4] Zhang C, Leighl NB, Wu YL and Zhong WZ. Emerging therapies for non-small cell lung cancer. J Hematol Oncol 2019; 12: 45.

[5] Yang CY, Yang JC and Yang PC. Precision management of advanced non-small cell lung cancer. Annu Rev Med 2020; 71: 117-36.

[6] Yang WC, Hsu FM and Yang PC. Precision radiotherapy for non-small cell lung cancer. J Biomed Sci 2020; 27: 82.

[7] Quintanal-Villalonga A, Chan JM, Yu HA, Pe'er D, Sawyers CL, Sen T and Rudin CM. Publisher correction: lineage plasticity in cancer: a shared pathway of therapeutic resistance. Nat Rev Clin Oncol 2020; 17: 382.

[8] Mellman I, Coukos G and Dranoff G. Cancer immunotherapy comes of age. Nature 2011; 480: 480-9.

[9] Pardoll DM. The blockade of immune checkpoints in cancer immunotherapy. Nat Rev Cancer 2012; 12: 252-64.

[10] Sharma P and Allison JP. The future of immune checkpoint therapy. Science 2015; 348: 56-61.
[11] Morad G, Helmink BA, Sharma P and Wargo JA. Hallmarks of response, resistance, and toxicity to immune checkpoint blockade. Cell 2021; 184: 5309-37.
[12] Gettinger SN, Horn L, Gandhi L, Spigel DR, Antonia SJ, Rizvi NA, Powderly JD, Heist RS, Carvajal RD, Jackman DM, Sequist LV, Smith DC, Leming P, Carbone DP, Pinder-Schenck MC, Topalian SL, Hodi FS, Sosman JA, Sznol M, McDermott DF, Pardoll DM, Sankar V, Ahlers CM, Salvati M, Wigginton JM, Hellmann MD, Kollia GD, Gupta AK and Brahmer JR. Overall survival and long-term safety of nivolumab (anti-programmed death 1 antibody, BMS-936558, ONO-4538) in patients with previously treated advanced non-small-cell lung cancer. J Clin Oncol 2015; 33: 2004-12.
[13] Thorsson V, Gibbs DL, Brown SD, Wolf D, Bortone DS, Ou Yang TH, Porta-Pardo E, Gao GF, Plaisier CL, Eddy JA, Ziv E, Culhane AC, Paull EO, Sivakumar IKA, Gentles AJ, Malhotra R, Farshidfar F, Colaprico A, Parker JS, Mose LE, Vo NS, Liu J, Liu Y, Rader J, Dhankani V, Reynolds SM, Bowlby R, Califano A, Cherniack AD, Anastassiou D, Bedognetti D, Mokrab Y, Newman AM, Rao A, Chen K, Krasnitz A, Hu H, Malta TM, Noushmehr H, Pedamallu CS, Bullman S, Ojesina AI, Lamb A, Zhou W, Shen H, Choueiri TK, Weinstein JN, Guinney J, Saltz J, Holt RA and Rabkin CS; Cancer Genome Atlas Research Network, Lazar AJ, Serody JS, Demicco EG, Disis ML, Vincent BG and Shmulevich I. The immune landscape of cancer. Immunity 2018; 48: 812-830, e14.
[14] Jiang P, Gu S, Pan D, Fu J, Sahu A, Hu X, Li Z, Traugh N, Bu X, Li B, Liu J, Freeman GJ, Brown MA, Wucherpfennig KW and Liu XS. Signatures of T cell dysfunction and exclusion predict cancer immunotherapy response. Nat Med 2018; 24: 1550-8.
[15] Brahmer JR, Tykodi SS, Chow LQ, Hwu WJ, Topalian SL, Hwu P, Drake CG, Camacho LH, Kauh J, Odunsi K, Pitot HC, Hamid O, Bhatia S, Martins R, Eaton K, Chen S, Salay TM, Alaparthy S, Grosso JF, Korman AJ, Parker SM, Agrawal S, Goldberg SM, Pardoll DM, Gupta A and Wigginton JM. Safety and activity of anti-PD-L1 antibody in patients with advanced cancer. N Engl J Med 2012; 366: 2455-65.
[16] Mok TSK, Wu YL, Kudaba I, Kowalski DM, Cho BC, Turna HZ, Castro G Jr, Srimuninnimit V, Laktionov KK, Bondarenko I, Kubota K, Lubiniecki GM, Zhang J, Kush D and Lopes G; KEYNOTE-042 Investigators. Pembrolizumab versus chemotherapy for previously untreated, PD-L1-expressing, locally advanced or metastatic non-small-cell lung cancer (KEYNOTE-042): a randomised, open-label, controlled, phase 3 trial. Lancet 2019; 393: 1819-30.
[17] Fehrenbacher L, Spira A, Ballinger M, Kowanetz M, Vansteenkiste J, Mazieres J, Park K, Smith D, Artal-Cortes A, Lewanski C, Braiteh F, Waterkamp D, He P, Zou W, Chen DS, Yi J, Sandler A and Rittmeyer A; POPLAR Study Group. Atezolizumab versus docetaxel for patients with previously treated non-small-cell lung cancer (POPLAR): a multicentre, open-label, phase 2 randomised controlled trial. Lancet 2016; 387: 1837-46.
[18] Yin X, Wang Z, Wang J, Xu Y, Kong W and Zhang J. Development of a novel gene signature to predict prognosis and response to PD-1 blockade in clear cell renal cell carcinoma. Oncoimmunology 2021; 10: 1933332.
[19] Chen Y, Li ZY, Zhou GQ and Sun Y. An immune-related gene prognostic index for head and neck squamous cell carcinoma. Clin Cancer Res 2021; 27: 330-41.
[20] Shen S, Wang G, Zhang R, Zhao Y, Yu H, Wei Y and Chen F. Development and validation of an immune gene-set based prognostic signature in ovarian cancer. EBioMedicine 2019; 40: 318-26.
[21] Ming J, Zhang Q, Qiu X and Wang E. Interleukin 7/interleukin 7 receptor induce c-Fos/c-Jun-dependent vascular endothelial growth factor-D up-regulation: a mechanism of lymphangiogenesis in lung cancer. Eur J Cancer 2009; 45: 866-73.
[22] Suzuki K, Kadota K, Sima CS, Nitadori J, Rusch VW, Travis WD, Sadelain M and Adusumilli PS. Clinical impact of immune microenvironment in stage I lung adenocarcinoma: tumor interleukin-12 receptor beta2 (IL-12Rbeta2), IL-7R, and stromal FoxP3/CD3 ratio are independent predictors of recurrence. J Clin Oncol 2013; 31: 490-8.
[23] Ming J, Jiang G, Zhang Q, Qiu X and Wang E. Interleukin-7 up-regulates cyclin D1 via activator protein-1 to promote proliferation of cell in lung cancer. Cancer Immunol Immunother 2012; 61: 79-88.
[24] Bonavita E, Gentile S, Rubino M, Maina V, Papait R, Kunderfranco P, Greco C, Feruglio F, Molgora M, Laface I, Tartari S, Doni A, Pasqualini F, Barbati E, Basso G, Galdiero MR, Nebuloni M, Roncalli M, Colombo P, Laghi L, Lambris JD, Jaillon S, Garlanda C and Mantovani A. PTX3 is an extrinsic oncosuppressor regulating complement-dependent inflammation in cancer. Cell 2015; 160: 700-14.
[25] Lin TY, Chan HH, Chen SH, Sarvagalla S, Chen PS, Coumar MS, Cheng SM, Chang YC, Lin CH, Leung E and Cheung CHA. BIRC5/Survivin is a

novel ATG12-ATG5 conjugate interactor and an autophagy-induced DNA damage suppressor in human cancer and mouse embryonic fibroblast cells. Autophagy 2020; 16: 1296-313.
[26] Wang Q, Zhu W, Xiao G, Ding M, Chang J and Liao H. Effect of AGER on the biological behavior of non-small cell lung cancer H1299 cells. Mol Med Rep 2020; 22: 810-8.
[27] Zhang Y, Cedervall J, Hamidi A, Herre M, Viitaniemi K, D'Amico G, Miao Z, Unnithan RVM, Vaccaro A, van Hooren L, Georganaki M, Thulin A, Qiao Q, Andrae J, Siegbahn A, Heldin CH, Alitalo K, Betsholtz C, Dimberg A and Olsson AK. Platelet-specific PDGFB ablation impairs tumor vessel integrity and promotes metastasis. Cancer Res 2020; 80: 3345-58.
[28] Liu Y, Zhang X, Yang B, Zhuang H, Guo H, Wei W, Li Y, Chen R, Li Y and Zhang N. Demethylation-induced overexpression of Shc3 drives c-raf-independent activation of MEK/ERK in HCC. Cancer Res 2018; 78: 2219-32.
[29] Li XY, Hou L, Zhang LY, Zhang L, Wang D, Wang Z, Wen MZ and Yang XT. OAS3 is a co-immune biomarker associated with tumour microenvironment, disease staging, prognosis, and treatment response in multiple cancer types. Front Cell Dev Biol 2022; 10: 815480.
[30] Parma B, Ramesh V, Gollavilli PN, Siddiqui A, Pinna L, Schwab A, Marschall S, Zhang S, Pilarsky C, Napoli F, Volante M, Urbanczyk S, Mielenz D, Schroder HD, Stemmler M, Wurdak H and Ceppi P. Metabolic impairment of non-small cell lung cancers by mitochondrial HSPD1 targeting. J Exp Clin Cancer Res 2021; 40: 248.
[31] Reda M, Ngamcherdtrakul W, Nelson MA, Siriwon N, Wang R, Zaidan HY, Bejan DS, Reda S, Hoang NH, Crumrine NA, Rehwaldt JPC, Bindal A, Mills GB, Gray JW and Yantasee W. Development of a nanoparticle-based immunotherapy targeting PD-L1 and PLK1 for lung cancer treatment. Nat Commun 2022; 13: 4261.
[32] Kim N, He N, Kim C, Zhang F, Lu Y, Yu Q, Stemke-Hale K, Greshock J, Wooster R, Yoon S and Mills GB. Systematic analysis of genotype-specific drug responses in cancer. Int J Cancer 2012; 131: 2456-64.
[33] Vokes NI, Chambers E, Nguyen T, Coolidge A, Lydon CA, Le X, Sholl L, Heymach JV, Nishino M, Van Allen EM and Janne PA. Concurrent TP53 mutations facilitate resistance evolution in EGFR-mutant lung adenocarcinoma. J Thorac Oncol 2022; 17: 779-92.
[34] Jia Y, Duan Y, Liu T, Wang X, Lv W, Wang M, Wang J and Liu L. LncRNA TTN-AS1 promotes migration, invasion, and epithelial mesenchymal transition of lung adenocarcinoma via sponging miR-142-5p to regulate CDK5. Cell Death Dis 2019; 10: 573.
[35] Murray PJ. Immune regulation by monocytes. Semin Immunol 2018; 35: 12-8.
[36] Worbs T, Hammerschmidt SI and Forster R. Dendritic cell migration in health and disease. Nat Rev Immunol 2017; 17: 30-48.
[37] Olivera A, Beaven MA and Metcalfe DD. Mast cells signal their importance in health and disease. J Allergy Clin Immunol 2018; 142: 381-93.
[38] Guo X, Zhang Y, Zheng L, Zheng C, Song J, Zhang Q, Kang B, Liu Z, Jin L, Xing R, Gao R, Zhang L, Dong M, Hu X, Ren X, Kirchhoff D, Roider HG, Yan T and Zhang Z. Global characterization of T cells in non-small-cell lung cancer by single-cell sequencing. Nat Med 2018; 24: 978-85.
[39] Jardim DL, Goodman A, de Melo Gagliato D and Kurzrock R. The challenges of tumor mutational burden as an immunotherapy biomarker. Cancer Cell 2021; 39: 154-73.